Progress In Electromagnetics Research C, Vol. 114, 43–56, 2021

A Compact Nonuniform Composite Right/Left-Handed Leaky-Wave Scanning Antenna with Elliptical Polarization for X-Band Application

Alexander Ostankov[1], Vladimir Kashkarov[2, *], and Evgeniy Khripunov[1]

Abstract—A new compact nonuniform leaky-wave antenna (LWA) with left-handed elliptical polarization (LHEP), based on composite right/left-handed (CRLH) metamaterial operating in the range of 7–10.2 GHz is presented in the work. The nonuniform structure of a CRLH transmission line (TL) is realized by the placement of different configurations of inter-digital capacitor (IDC) in the form of sinusoid (SIN-IDC), on the top of metal wall of a half-mode substrate integrated waveguide (HMSIW). Balanced condition of the unit cells is provided by the change in slit width, amplitude, and the number of SIN-IDC periods, as well as by relocation of two additional transition apertures arranged by both sides of SIN-IDC. Based on the known Hensen-Woodyard criterion, the optimal number of the unit cells was determined, when the gain coefficient varied from 7.5 to 9.8 dB in all of the operational range of antenna. The developed prototype of nonuniform CRLH LWA has the size of 8.1×115.2 mm. It is characterized by a continuous scan angle range equal to 117°. The maximum angle of rotation radiation pattern is −66° for backward radiation and +51° for direct radiation. The maximum efficiency of the antenna radiation is 85%, while the total one is 68%.

1. INTRODUCTION

With the appearance of transmission lines (TLs), prepared by the substrate integrated waveguide technology (SIW) [1, 2], preserving the main advantages of the bulk waveguides under low height and weight of the substrate, a lot of various leaky-wave antennas (LWAs) appeared. LWAs on the basis of SIW are distinguished by a high gain, narrow beam width, excellent scanning-frequency characteristics, and high performance. However, unidirectional periodic LWAs based on TLs composed only of the materials with positive (right-handed — RH) or negative (left-handed — LH) permeability μ and permittivity ε, including those ones produced by SIW-technology, have certain limitation. It is associated with the occurrence of open-stopband (OSB) near the direction of radiation that is normal to the antenna aperture [3]. For the periodic SIW and half-mode substrate integrated waveguide (HMSIW) LWAs (period of unit cell $\sim \lambda_g$), several methods for the suppression of OSB were proposed: the use of impedance-matched unit cell [4], properly adjusting the structure parameters of the slots in unit cell [5], and asymmetric technique [6]. However, a lot of periodic LWAs have been described in literature in spite of that they demonstrated high gain and low side lobe level (SLL), but they have much greater dimensions in the direction of the electromagnetic waves propagation and cover less scanning sector than LWAs based on the composite right-/left-handed (CRLH) TLs [7].

CRLH TL structure combines RH and LH effects. Thereby, it represents construction based on metamaterials composed of periodically arranged inductances and capacitances in the unit-cell of TL

Received 31 May 2021, Accepted 6 July 2021, Scheduled 17 July 2021

* Corresponding author: Vladimir Kashkarov (vmkashkarov@gmail.com).

[1] Radio Engineering Department, Voronezh State Technical University, Moskovsky pr-t, 14, Voronezh, Russia. [2] Solid State Physics and Nanostructures Department, Voronezh State University, Universitetskaya pl.1, Voronezh, Russia.

[8]. In [9–12], various CRLH LWAs were presented (period of the unit cell $< \lambda_g/4$), employing all of the advantages of SIW-technology, where OSB was suppressed by attainment of the balanced condition of the unit cell. Thus, a wide scanning angle was provided in both directions. Data on the compact LWA based on SIW with circularly polarization (CP), operating in X-band are presented in [9]. A SIW leaky-wave structure for polarization-flexible antenna application was proposed in [10]. The development of SIW LWA from nonuniform CRLH unit cells with SLL reduction was employed in [11]. A structure of CRLH TL unit cell in [9–11] was provided by the arrangement of the series interdigital capacitor (IDC) in the form of a meander type slot line on the top wall of SIW. A miniature frequency-scanning HMSIW LWA with CP was reported in [12]. Ramp-shaped slots here were employed as a series IDC.

According to the results of previous investigations, the highest gain and at the same time low-level SLL and a small radiator length demonstrated nonuniform CRLH [11] and nonuniform periodic LWAs based on SIW [13]. However, their lateral dimension can be considerably diminished in the case of HMSIW use. Therefore, the main idea of the work is in the development of a compact nonuniform CRLH LWA on the basis of HMSIW with elliptical polarization (EP) or CP, which is capable to scan in the forward direction as in the backward direction (including transversal one) with a continuous beam. To design a nonuniform CRLH LWA structure, providing EP, and, in particular, CP, it is proposed to use three unit cells with different configurations of series IDC in the form of sinusoid (SIN-IDS), arranged at the top metal wall of HMSIW. Two additional plated vias are also specified in the design of unit cells arranged by both sides of SIN-IDC. This approach makes it possible to control parameters of the structure in easier way thus making the tuning of antenna structure faster. The developed nonuniform LWA is compared with those presented in the previous works. As far as it is known to the authors, this design of CRLH unit-cells was not previously considered in literature. The ready specimen of LWA consists of three different stages involving 12 balanced CRLH unit cells, and it is tested with the use of network analyzer Rhode&Schwarz ZVL13.

2. PROPOSED CRLH UNIT-CELLS DESIGN AND ANALYSIS

2.1. CRLH Unit-Cells Based on HMSIW with SIN-IDC

HMSIW can be regarded as one of the most advantageous structures from the viewpoint of usability and compactness for the design of CRLH unit cells and LWA on the basis of these structures. If HMSIW is considered as a two-wire transmission line (TL), then its top metal wall can be interpreted as a distributed in series inductance L_R, while the dielectric packaged between the top and grounded surfaces as the parallel capacitance C_R. These elements of the construction support a direct propagation of electromagnetic wave and provide radiation in the range of RH. The plated vias that correspond to the metal wall of the waveguide represent the distributed parallel inductance L_L. Thus, in order to design CRLH unit-cells, which can also support a backward propagation of the waves and, correspondingly, radiation in LH region, cannot attain only a series capacitance C_L; several configurations of SIN-IDC were proposed to be used as this capacitance.

The overall view and basic sizes of CRLH unit cells are depicted in Fig. 1(a) with a cell for the first stage of LWA. Figs. 1(b)–1(d) demonstrate configurations and dimensions of SIN-IDC, and the offset of additional plated vias for the first, second, and third stages of antenna, respectively. The main difference between the unit cells is in the extent of SIN-IDC in the direction of HMSIW, which is determined by parameter a_{slot}. In order to make CRLH unit cells on the basis of HMSIW a Rogers RO4003C substrate was chosen with the permittivity of $\varepsilon_r = 3.38$, dielectric loss tangent $tg_s = 0.0027$, and thickness $h = 0.508$ mm. From theoretical viewpoint, the length or period of arrangement for unit-cells p is chosen with the account of the metamaterial structure uniformity, and it should be rather small (generally $p < \lambda_{\mathrm{g}}/4$, where λ_{g} is a wavelength in the guiding structure of TL) [14]. However, by controlling the value of parameter p within the permissible limits it is possible to change the slope of the air-line ($k_0 p/\pi$) and thus to move position of the region for the fast/slow waves. The width of the prominent part of HMSIW g_{hmsiw}, which has only bottom metallization layer, is determined on the ground of reducing the side lobe levels and, hence, improvement of antenna gain.

Since polarization of the ready LWA is dependent on the value and direction of the surface currents flow J_s in the structure of the unit cell, it is important to choose the correct form of IDC or its arrangement at TL. In order that the developed nonuniform CRLH LWA would provide EP or CP

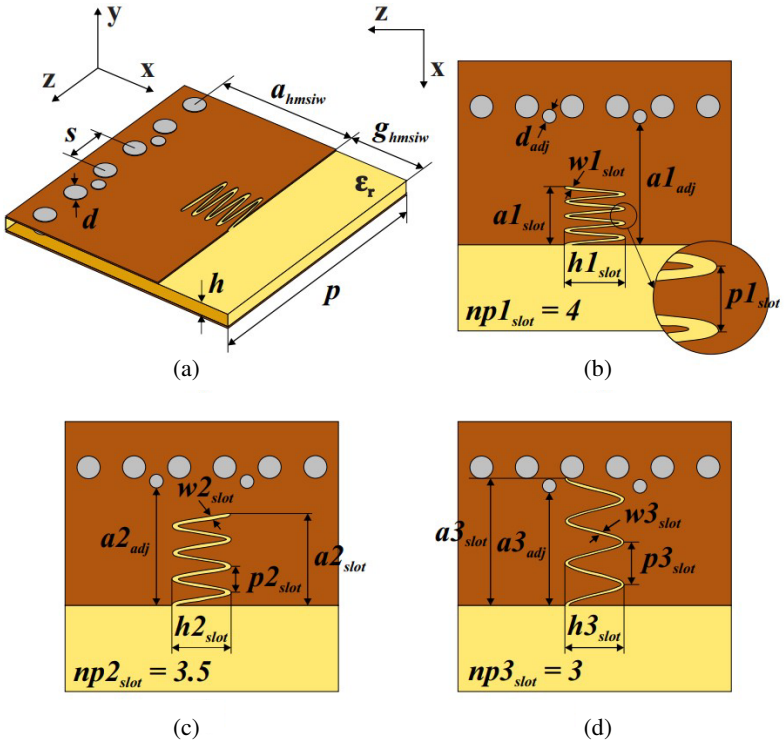

Figure 1. CRLH unit-cells based on HMSIW: (a) overall view and basic sizes, (b)–(d) SIN-IDC configurations and offset of the additional plated vias for three antenna stages.

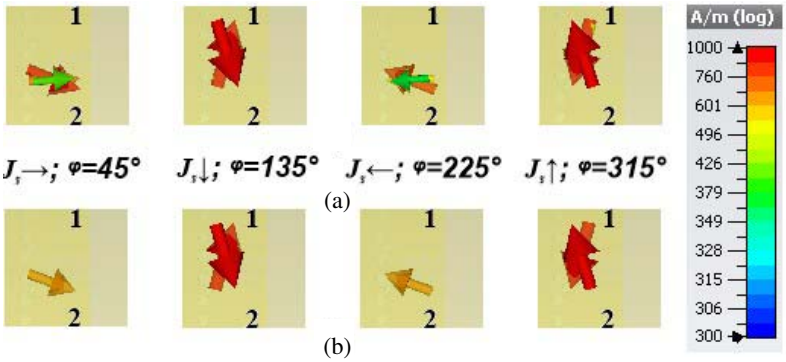

Figure 2. Direction of the surface current J_s in the unit cell of the first stage for different values of signal phase φ: (a) in the range of LH ($f = 7.8\,\text{GHz}$), (b) in the range of RH ($f = 8.5\,\text{GHz}$).

polarization, and balancing of the unit cells would be flexible, but it takes little time, authors of this work propose to employ IDC in the form of sinusoid — SIN-IDC. The directions and amplitudes of the surface currents J_s, passing through the structure of the unit cell, are presented in Fig. 2. These values were measured in the equal intervals of time $\tau = n \cdot t/4$, where τ is a period of signal and $n = 1, 2 \ldots 4$. In CST program suite these selected time intervals τ are associated with the values of phase $\varphi = 45°$, 135°, 225°, and 315°. Note that while the exciting signal crosses central frequency f_0, plane-of-polarization rotation can change. Therefore, the amplitudes and directions of the currents J_s in Fig. 2(a) are depicted for LH region ($f = 7.8\,\text{GHz}$), while the same for RH region ($f = 8.5\,\text{GHz}$) is shown in Fig. 2(b). The measurements were performed for configuration of the unit cell corresponding to the second stage of LWA. As it is seen from Fig. 2, if the excitation of the unit-cell is implemented through port No. 1 (designated by number 1 in Fig. 2), then on both of the regions (LH and RH), the

main current J_s is rotated clockwise. Then, it follows that if the direction of the excitation for the fabricated LWA coincides with the direction of excitation for the unit cell from port No. 1, then antenna is featured as left-handed EP (or CP) [15]. On the contrary, if the excitation direction of antenna is co-directional with the excitation of the unit cell from port No. 2, then rotation of polarization plane is changed in the opposite direction.

The balanced condition of the unit cell means that when the resonance frequencies of series f_{se} and parallel f_{sh} connected loops are equal: $L_R C_L = L_L C_R$, then contributions of the areas LH and RH are completely balanced at some central frequency f_0, calculated based on Equation (1) [14]:

$$f_0 = \frac{1}{2\pi\sqrt[4]{L_R C_R L_L C_L}} = \frac{1}{2\pi\sqrt{LC}} \tag{1}$$

In accordance with the proposed CRLH unit cells, balanced condition was provided by the changes of the following SIN-IDC parameters: number of the periods np_{slot}, width of the slot w_{slot}, and span h_{slot}, as well as by the width of HMSIW a_{hmsiw} and offset of the additional plated vias a_{adj}.

2.2. Analysis of Dispersion Characteristics

For search of the balanced condition in the proposed CRLH unit-cells and performing estimation of the operation range for nonuniform LWA, respectively, the analysis of their dispersion characteristics was executed. Equivalent models of the unit-cells, taking into account their real physical dimensions were designed in the software suite CST Microwave Studio. While periodical conditions are performed for the unit-cell at each stage and in order to exclude the impact of mutual coupling between them a simulation was done using frequency-domain solver (which operates much faster than with the use of eigen-mode solver [12]); as a result, the required S-parameters were extracted. Excitation of the unit-cells was employed with the use of waveguide ports. The curves of dispersion characteristics β and α, depicted in Figs. 3(a)–3(d), were obtained by substituting the found S-parameters values into the following expressions [9, 11]:

$$\beta p = \mathrm{Re}\left[\cos^{-1}\left(\frac{1 - S_{11}S_{22} + S_{12}S_{21}}{2S_{21}}\right)\right] \tag{2}$$

$$\alpha p = \mathrm{Re}\left[\cosh^{-1}\left(\frac{1 - S_{11}S_{22} + S_{12}S_{21}}{2S_{21}}\right)\right] \tag{3}$$

where p is the length or period of the unit-cells, β the phase constant, and α the attenuation constant.

Dispersion curves for the unbalanced CRLH unit-cell at the second stage of LWA are presented in Figs. 3(a) and 3(b). As one can see, within the frequency range where LWA steers scanning beam strictly vertically or close to this direction, an open stop-band (OSB) is observed since the ratio of α/k_0 is greater than β/k_0 ($\alpha/k_0 > \beta/k_0$). Such a loss in efficiency of LWA can be explained by Bragg diffraction, and this confirms that $f_{se} \neq f_{sh}$. Note that in the first case (Fig. 3(a)) $f_{se} < f_{sh}$, while in the second one (Fig. 3(b)) $f_{se} > f_{sh}$. While approaching the balanced condition, shown in Fig. 3(c), a decrease of OSB takes place, and it means that the frequency range, where $\alpha/k_0 > \beta/k_0$, gets gradually narrowed. When parameters of SIN-IDC and HMSIW width become equal: $h2_{slot} = 2\,\mathrm{mm}$, $np2_{slot} = 3.5\,\mathrm{mm}$, $a_{hmsiw} = 4.9\,\mathrm{mm}$, series f_{se} and parallel f_{sh} resonances balance each other implying balanced condition of the unit cell. In this case, a smooth transition from LH region to RH one proceeds at the central frequency of $f_0 = 8\,\mathrm{GHz}$, determined according to Equation (1). This effect is reduced to minimum manifestation of Bragg diffraction. Even in the case when $\beta = 0$, radiation can be observed since the group velocity $v_g \neq 0$. It should be noted that the decay constant α within the ranges from 7 to 9.4 GHz and from 9.8 to 11.4 GHz is relatively small and is characterized by the uniform distribution.

Curves of dispersion characteristics for the balanced CRLH unit cells of all three LWA stages are depicted in Fig. 3(d). One can see that with an increase of parameter a_{slot}, responsible for the length of SIN-IDC in the lateral direction of HMSIW, an increase of the operation range is observed in LH region. Therefore, the basis of nonuniform LWA should be composed of the cells at the third stage. All of the dimensions for the balanced CRLH unit cells, used for providing of the dispersion curves in Fig. 3(d), are presented in Section 4 (Table 1).

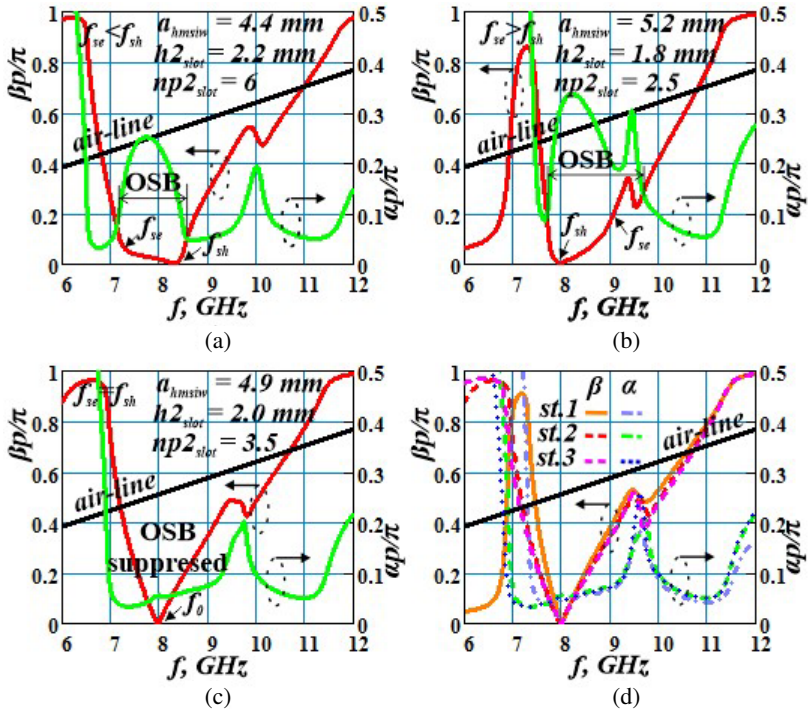

Figure 3. Curves β and α of the dispersion characteristics, calculated for CRLH unit cell at the second stage of LWA: unbalanced condition (a) and (b), balanced (c); calculated for the balanced CRLH unit cells of all three LWA stages (d).

3. ANALYSIS BASED ON THE EQUIVALENT CIRCUIT IN AWR

Along with full-wave simulation in CST suite software CRLH unit-cell analysis of the second stage of LWA was performed in AWR suite software basing on its equivalent circuit presented in Fig. 4. In this case, dispersion characteristics were optimized by selection of the corresponding elements. In particular, series inductance L_{hmsiw} is coupled with the period of repetition or the length of cell p. Capacitance C_{hmsiw} parallel to this inductance corresponds to the type of the employed substrate, since it depends

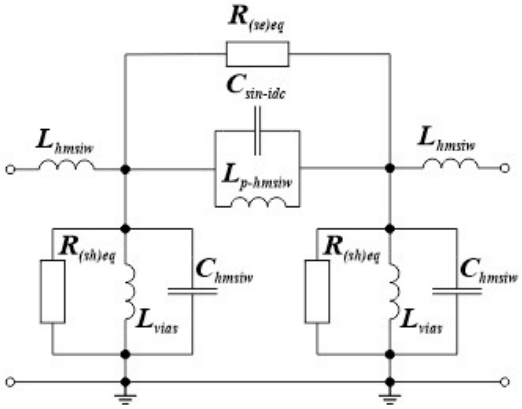

Figure 4. Equivalent circuit for CRLH unit cell of the second stage of LWA. Values of the elements for the balanced condition: $L_{hmsiw} = 1.4\,\text{nH}$, $C_{hmsiw} = 1.13\,\text{pF}$, $L_{vias} = 0.4\,\text{nH}$, $C_{sin-idc} = 1.23\,\text{pF}$, $L_{p-hmsiw} = 0.5\,\text{nH}$, $R_{se(eq)} = 5\,\text{kOhm}$, $R_{sh(eq)} = 1\,\text{kOhm}$.

on the value of its dielectric permeability $\varepsilon\varepsilon_r$, its height h, and its width a_{hmsiw}. Inductance of L_{vias} is set in a dependence of the chosen size of the main and additional plated vias and their number. Series capacitance $C_{sin-idc}$ involves the main parameters of SIN-IDC: the number of periods np_{slot}, width of the slot w_{slot}, span h_{slot}, and length a_{slot}. To represent the balance between the layer of HMSIW metallization, which lies just above SIN-IDC, and the length of SIN-IDC itself, a parasitic inductor $L_{p-hmsiw}$ is mounted parallel to the capacitor of $C_{sin-idc}$. Resistors $R_{se(eq)}$ and $R_{sh(eq)}$ determine the total equivalent impedance of the circuit.

In order to characterize an impedance of CRLH unit-cell in the periodic TL, one can use Bloch impedance Z_B, which can be determined on the basis of the following expression [16]:

$$Z_B = \pm Z_0 \sqrt{\frac{(1+S_{11})^2 - S_{21}^2}{(1-S_{11})^2 - S_{21}^2}} \tag{4}$$

where Z_0 is a characteristic impedance of TL.

Varying the values of the elements C_{hmsiw} and $C_{sin-idc}$ of equivalent circuit, one can determine an impact of parameters SIN-IDC and the width of HMSIW on the curve β of dispersion characteristics and Bloch impedance Z_B. Curves β and $\mathrm{Re}(Z_B)$, depicted in Figs. 5(a)–5(c), were calculated by the substitution of S-parameters, obtained in AWR simulation into Equations (2) and (4).

If C_{hmsiw} is less and $C_{sin-idc}$ greater than the value providing balanced condition of the equivalent circuit for the specified central frequency (Fig. 5(a)), then $f_{se} < f_{sh}$; curve β within the range of 7.4 – 8.5 GHz demonstrates clearly expressed OSB, and at the frequency equal to f_{se} a sharp increase of $\mathrm{Re}(Z_B)$ up to $\sim$ 90 Ohms is observed. This state of the circuit corresponds to CRLH unit-cell configuration at the second stage of LWA shown in Fig. 3(a); it means that the width of HMSIW a_{hmsiw} is needed to be increased while the number of periods $np2_{slot}$ and the span of $h2_{slot}$ SIN-IDC, vice versa, are to be reduced. In the opposite case when C_{hmsiw} is greater and $C_{sin-idc}$ less than the required values (Fig. 5(b)), $f_{se} > f_{sh}$; OSB becomes much narrower, and it is within the range of 7.7–8.4 GHz. A sharp increase of $\mathrm{Re}(Z_B) > 100$ Ohm is at the frequency of f_{se} as before. This case

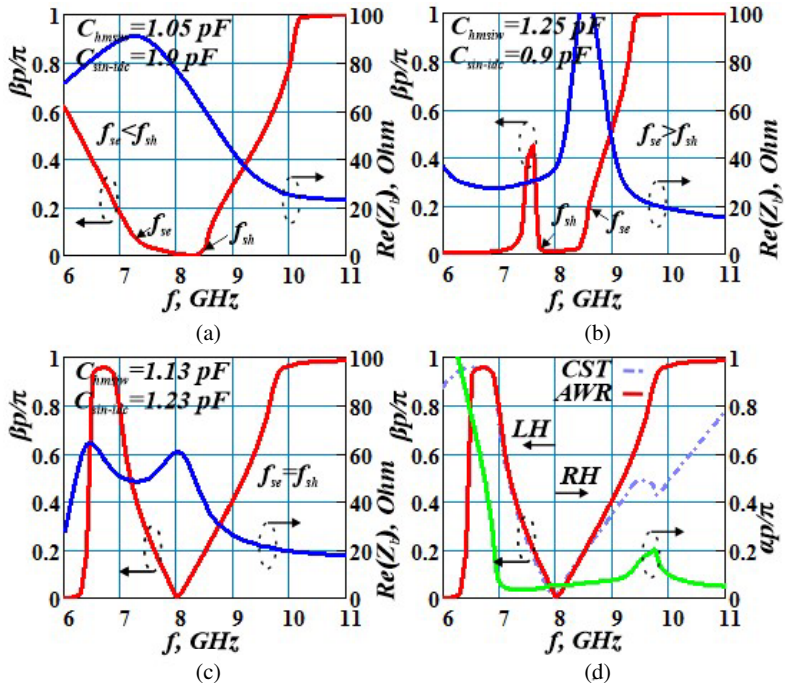

Figure 5. Curves of dispersion characteristics β and real part of Bloch impedance $\mathrm{Re}(Z_B)$, calculated with the help of equivalent circuit in AWR for CRLH unit cell of the second LWA stage: unbalanced condition (a) and (b), balanced condition (c); comparison of the curves β of the dispersion characteristics for balanced CRLH unit-cell in CST and AWR software suites.

represents CRLH unit cell configuration in Fig. 3(b), and it implies the necessity in a decrease of HMSIW a_{hmsiw} width and increase of the number of periods $np2_{slot}$ as well as the span of $h2_{slot}$ SIN-IDC. When $f_{se} = f_{sh}$, the equivalent circuit (Fig. 4) represents the balanced condition of CRLH unit cell at the second stage of LWA (Fig. 5(c)). So at the frequency of transition $f_0 = 8$ GHz a smooth changeover of the dispersion characteristics β from the region of LH to that one of RH occurs, while OSB is completely suppressed. The curve $\mathrm{Re}(Z_B)$ monotonously increases from 50 to 70 Ohm in LH region (7–8 GHz) and then monotonously decreases up to 20 Ohm as well in the region of RH (8–9.7 GHz).

For comparison, curves β of the dispersion characteristics, obtained in CST software suite (Fig. 3(c)) and with the help of the equivalent circuit in AWR software suite (Fig. 5(c)) for the balanced CRLH unit-cell, are presented in Fig. 5(d). As it is seen, curve β is obtained with full-wave simulation in CST software suite, where the real physical dimensions of CRLH unit cell are considered, and β, calculated with the use of equivalent circuit in AWR software suite, is very similar. However, in the second case an impact of magnetic wall is not taken into account, and this can explain some differences between them.

4. NON-UNIFORM CRLH LWA DESIGN

Just as the other types of similar CRLH LWAs, the proposed antenna is realized by a sequential arrangement of the balanced unit-cells along z axis with periodicity of p. Unlike periodic LWAs, where radiation passes through a spatial harmonic (mainly $n = -1$) for LWAs consisting of CRLH unit-cells, it is performed due to the basic mode of the guiding TL structure ($n = 0$) [17]. The analysis done previously for the dispersion characteristics of CRLH unit-cells demonstrates that the developed LWA is characterized by LHEP and performs scanning within the range of 7 to 10.7 GHz and with a central frequency of $f_0 = 8$ GHz. It should be noted that the scanning range was determined by the results of simulation for CRLH unit cell of the third stage LWA since it is the basis for the nonuniform structure of antenna. Fig. 6(a) represents the overall view of the developed nonuniform CRLH LWA and its basic dimensions which are also given in Table 1. Fig. 6(b) represents a photo of the made antenna specimen.

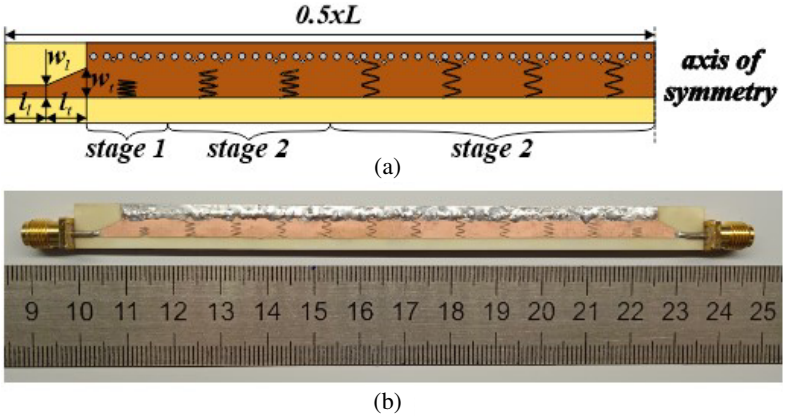

(a)

(b)

Figure 6. The proposed non-uniform CRLH LWA: (a) basic dimensions, (b) photo of the prepared sample comprised in total of 12 unit cells (2-unit cell — stage 1, 4 — stage 2, 6 — stage 3).

In order to transfer energy to HMSIW structure and its matching with the other elements of the terminal device connection of 50-Ohm load, two micro-strip joints are utilized arranged by both sides of LWA [18]. These joints consist of 50-Ohm transmission lines and tapered quarter-wave transformers connected directly to the upper metal wall of HMSIW.

The curves of the maximal gain in dependence on frequency in Fig. 7(b) were obtained for LWAs with different lengths, which is determined by the number of the unit cells. Dependences of the maximum for side lobes level on the frequencies in Fig. 7(a) were obtained for LWAs with different configurations of the radiator, which is composed of the unit cells of all three stages.

According to Hansen-Woodyard test [19], maximum directivity of the travelling wave antenna attaining the phase difference between the surface wave and the wave in the free space is equal to 180°.

Table 1. Basic dimensions of non-uniform CRLH LWA.

Par.	Value, mm	Par.	Value, mm	Par.	Value, mm	Par.	Value, mm	Par.	Value, mm
p	9.6	$a1_{\text{adj}}$	4.55	$a2_{\text{adj}}$	4.4	$a3_{\text{adj}}$	4.25	L	115.2
a_{hmsiw}	4.9	$w1_{\text{slot}}$	0.085	$w2_{\text{slot}}$	0.105	$w3_{\text{slot}}$	0.09	w_{t}	3.5
g_{hmsiw}	3	$h1_{\text{slot}}$	2.1	$h2_{\text{slot}}$	2	$h3_{\text{slot}}$	2	l_{t}	5
s	1.6	$a1_{\text{slot}}$	2.05	$a2_{\text{slot}}$	3.275	$a3_{\text{slot}}$	4.5	w_{l}	1.14
d	0.8	$p1_{\text{slot}}$	0.5125	$p2_{\text{slot}}$	0.9357	$p3_{\text{slot}}$	1.5	l_{l}	5
d_{adj}	0.5	$np1_{\text{slot}}$	4	$np2_{\text{slot}}$	3.5	$np3_{\text{slot}}$	3	h	0.508

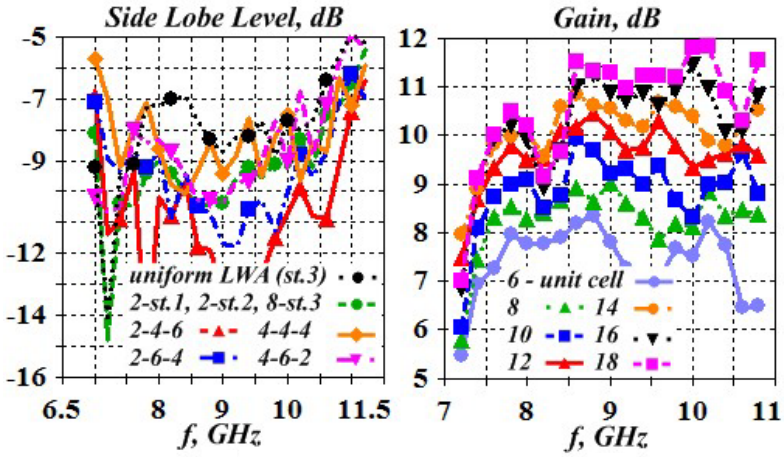

(a) (b)

Figure 7. (a) Curves of the maximum SLL for some configurations of nonuniform LWA structure, composed of different CRLH unit cells for three antenna stages. (b) Curves of the maximum LWA gain, composed of the different numbers of CRLH unit cells for the third (main) stage.

In [20], there are also confirmed data that the original model of Hansen-Woodyard can be applied to LWA and provide quite optimal results.

On the basis of the results in Fig. 7(b), the largest directivity of LWA is attained for the radiator length of $L = 115,2\,\text{mm}$ ($\sim 3.07\lambda_0$) without taking account of the matching transitions, and it consists of 12 unit cells. Under further increase of their number, the gain is also raised but in much less degree. This small increase can be due to the insignificant enhancement of LWA efficiency. Therefore, in order to keep compactness of antenna and do not rise in cost of its production, it seems optimal to make a radiator composed of 12 CRLH unit-cells.

As one can see from Fig. 7(a), the lowest SLL in a nonuniform LWA structure can be observed for the configuration composed of two unit cells of the first stage, four cells of the second one, and six cells of the third stage.

5. COMPARISON OF SIMULATION AND MEASUREMENT RESULTS AND DISCUSSION

Transmission gain S_{21} and reflection factors S_{11} of the proposed nonuniform CRLH LWA, obtained in the full-wave simulation with the use of frequency-domain solver in software CST suite and those ones measured with the network analyzer Rohde & Schwarz ZVL13, are presented in Fig. 8. Differences between the results are associated with different reasons. First, the losses in the conductor and dielectric

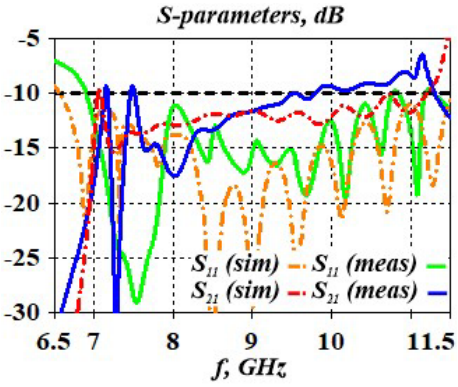

Figure 8. Simulated and measured S-parameters of non-uniform CRLH LWA.

are usually higher in the measurement process. Second, losses in SMA connectors were not taken into account in the simulation. Third, the process of antenna production was not implemented in the manufacturing environment but was employed as a chemical etching of the substrate. Therefore, geometry of some SIN-IDC is quite noticeably disturbed, and it does not have a distinguished boundary with the conductor. This, in turn, can provide an additional shift of the operating range of LWA and thus increase the losses in the conductor.

In order to represent the operating range of antenna, where the power leaking from the TL structure would be associated rather with just the radiation but not with the reflection from the port or its transfer from port to port, it is required that S_{21} and S_{11} would be less than -10 dB. So, the bandwidth for the impedance matching was 7 to 11,2 GHz as compared with the simulation results (52.5%) and from 7 to 10.2 GHz according to the results of measurements (40%).

Axial Ratio (AR) of the main beam of radiation pattern ($\varphi = 90°$, $\theta = \theta_m^\circ$) dependent on the frequency obtained in the simulation in software CST suite is depicted in Fig. 9. To obtain sufficient circular polarization, it is required that AR should be less than 3 dB, and phase difference of the two orthogonal components stipulating circular polarization should be close to 90°. Thus, the developed antenna demonstrated an expressed elliptical polarization (EP) over the whole operational range of frequencies. The values of AR that are closest to CP (< 6 dB) are observed for the main beam in the range of LH from 7.4 to 7.6 GHz.

Figure 10 demonstrates dependence of the direction for the main beam of radiation pattern (RP) on frequency. One can see that the developed nonuniform CRLH LWA provides a continuous sector of the scanning angles equal to 129° in simulation and equal to 117° during the measurements. The maximum angle of rotation for RP measured from the normal is of $-56°$ in the first case (for back-scattered radiation) and $+73°$ (for direct radiation), while in the second case these angles are $-66°$

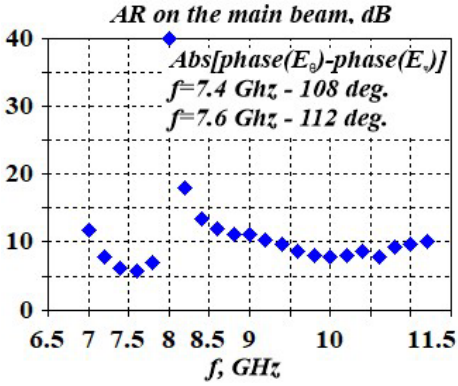

Figure 9. Axial Ratio on the main beam radiation pattern.

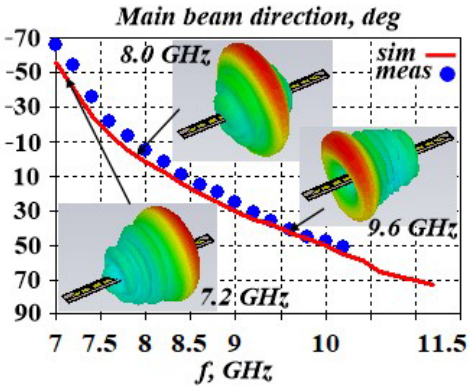

Figure 10. Direction of the maximum for the main beam in a dependence of frequency and 3D-models of the antenna patterns.

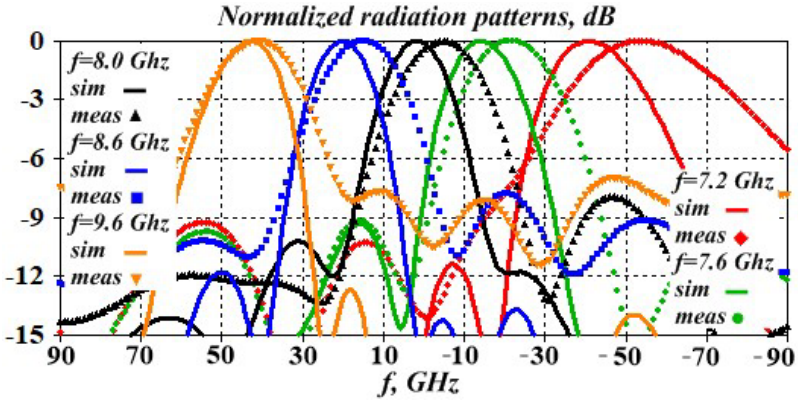

Figure 11. Simulated and measured normalized antenna patterns.

and +51°, respectively. Note that measurement of the ready antenna specimen was performed up to the frequency of 10.2 GHz, where transmission gain S_{21} is raised above −10 dB, and matching of the structure impedance deteriorates. Therefore, the maximum angle of rotation for RP in the RH region during the measurements is considerably less. One more difference between the results is in the shift of frequency that is of +200 MHz for the central frequency $f_0 = 8$ GHz. Such a shift is due to the effect of real losses (in the connectors as a result of non-ideal load matching) and deviations of the overall dimensions of SIN-IDC from the calculated ones during the fabrication.

3D-models of RP obtained as a result of simulation are also presented in Fig. 10. According to their images, it is seen that for the frequencies below the transition value ($f < f_0$), LWA radiates back-scattered beam (directed towards the source of radiation), and CRLH structure provides operation in LH region. At the transition frequency ($f_0 = 8$ GHz), the beam is directed actually vertically ($\theta_m \approx 90°$), while the radiation occurs because the group velocity v_g proves to be non-zero. Above the transition frequency ($f > f_0$), CRLH structure provides operation in RH region, while the scanning beam is directed straightforward (relative to the source of excitation).

Normalized LHCP radiation patterns in E-plane (y-z), obtained in the process of simulation and by the measurements, are depicted in Fig. 11. As it was previously assumed, if the antenna is excited from the right port (Fig. 6(b)), then the polarization corresponds to LHCP, while cross-polarization is associated with RHCP, since in both cases its level was below 12 dB. If the power is supplied from the opposite port, then rotation of the polarization is changed to the inverse one.

Curves of the maximum gain value are presented in Fig. 12. Its greatest level in the simulation process was attained at the frequency of 9 GHz, and it is equal to ∼ 10.1 dB. In the measurements its maximum value is by ∼ 0.3 dB less than the results of simulation, and moreover, it is shifted towards

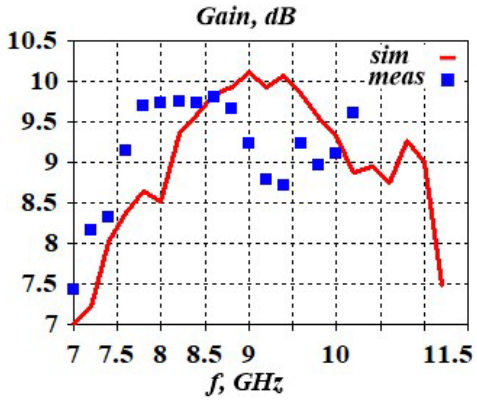

Figure 12. Simulated and measured gain coefficient of LWA.

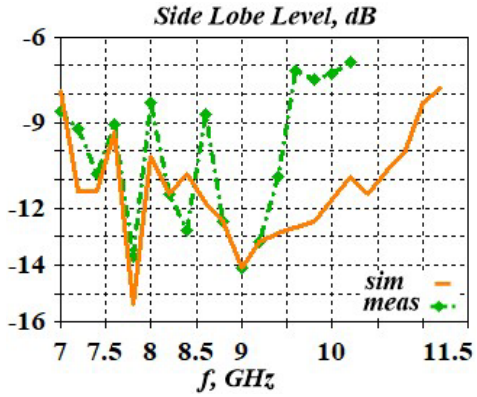

Figure 13. Simulated and measured maximum level of SLL.

LH region by 400 MHz. Since both curves do not show significant dips at the transition frequency (f_0 = 8 GHz and 8.2 GHz), one can state that the efficiency of the RP is kept for strictly vertical direction of the main beam. It should also be noted that the presented and simulated maximum gain values are in a good agreement with those of LHCP RPs levels (Fig. 11), obtained before the normalization procedure. This permits once again to confirm the correctness of determination for co-polarization and cross-polarization.

while feeding the antenna from the right port antenna has LH polarization, while feeding from the opposite side will be RH polarization

Simulated maximum value of SLL, presented in Fig. 13, does not exceed −10 dB actually all over the operation range excluding extreme frequencies, while the measured one is no more than −8 dB. The lowest values of SLL in the regions of LH and RH are provided at the frequencies of 7.8 and 9 GHz, and they are below −14 dB. Radiation efficiency of antenna calculated in software CST suite, presented in Fig. 14, within the range of 7.2–10.2 GHz varies within 70 to 85%, while the overall efficiency is more than 48%.

Table 2 provides the main characteristics of several periodic and CRLH LWAs, fabricated with the use of SIW technology, which are presented for comparison with the proposed nonuniform CRLH LWA. In the case when information in the source reference was not in the explicit form, the data obtained from the presented figures and tables in the source are introduced in the Table 2. If there was no any information, then it was recorded as Non-Available (N/A). For the length of antenna radiator L, given without taking account of the feed line, the value relative to the wavelength in the free space λ_0 taken at the transition frequency f_0 is presented in parenthesis. Working bank frequency is also presented in percentage terms relative to f_0.

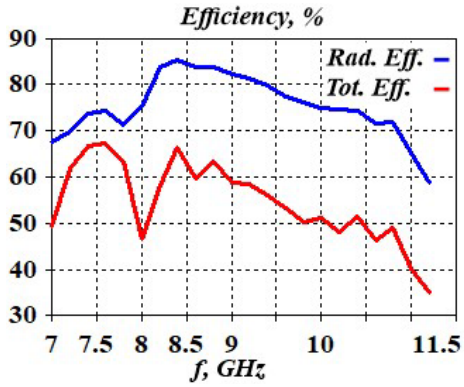

Figure 14. Efficiency of LWA radiation calculated in software CST suite and the overall efficiency.

Table 2. Comparison of SIW and HMSIW LWA characteristics.

Ref.	**Type and technology of LWA (type of slot or IDC)**	**Pol.**	**Size of radiator without feed line W*L ($L \times \lambda_0$), mm**	**BW, GHz (relatively f_0, %)**	**Scan range, °**	**Min SLL, dB**	**Peak Gain, dB**	**Max Rad. Eff.; Tot. Eff., %/%**
[5]	Periodic HMSIW (Transverse slots with a combination of two arrow shaped slots)	LP	16×147 ($6.84\lambda_0$)	10–16.5 (46.36)	−50° to 26° (76°)	∼ (−12)	∼12	N/A; N/A
[6]	Periodic SIW (Asymmetric double slot)	N/A	14.5×187 ($9.1\lambda_0$)	12.6–16.2 (24.66)	−32° to 27° (59°)	∼ (−15)	∼12.5	∼85*; N/A
[9]	CRLH SIW (T-shaped IDC as meander type slot line)	CP	17.8×130.1 ($3.25\lambda_0$)	7.35–10.15 (32)	−19° to 84° (103°)	∼ (−8)	∼8.95	∼96; N/A
[11]	Non-uniform CRLH SIW (Three configuration IDC as meander type slot line)	LP	N/A×172.2 ($5.74\lambda_0$)	9–13.4 (44)	−52° to +64° (116°)*	∼ (−20)*	∼15*	∼95*; N/A
[12]	CRLH HMSIW (IDC as ramp-shaped slots)	CP	12×160 ($4.8\lambda_0$)	7.4–13.5 (67.8)	−70° to 70° (140°)	∼ (−10)	∼12	N/A; N/A
This work	**Non-uniform CRLH HMSIW (Three configuration IDC as sinusoidal slot — SIN-IDC)**	**EP**	**8.1×115.2 ($3.07\lambda_0$)**	**7–10.2 (40)**	**−66° to 51° (117°)**	**∼(−14)**	**∼9.8**	**85*/68***

*Simulated results

6. CONCLUSION

A compact nonuniform CRLH LWA with EP was developed and implemented on the basis of HMSIW. In order to create a CRLH TL structure and EP-radiation, three unit-cells were utilized with different configurations of IDC in the form of sinusoid – SIN-IDC, arranged at the top metal wall of HMSIW. The main difference between the unit-cells was in the lateral extent of SIN-IDC, the number of its periods, the value of its span, slot width, as well as in the place of a set of two additional plated vias arranged by both sides of SIN-IDC. For all of the unit-cells, their balanced condition in the process of simulation was provided at the central frequency of 8 GHz. Measurements made with the fabricated specimen composed in total from 12 balanced unit cells (2 — stage 1, 4 — stage 2 and 6 — stage 3) and having dimensions of 8.1×115.2 mm without the account of the feed line showed that the developed antenna provided operation all over the range of X-band (7–10.2 GHz), and it has wide continuous angular domain of scanning equal to 117°. The maximum angle of rotation for the directivity pattern in the region of LH is −66°, while for RH region it is +51°. OSB suppression is provided at the frequency of 8.2 GHz (+200 MHz relative to simulation) since just at this value the main beam is strictly vertical. This shift is caused by the errors while fabrication of the prototype and the effect of the actual losses (in the connectors or due to non-ideal load matching). The maximum measured gain was 9.8 dB at the frequency of 8.6 GHz. The lowest values of SLL in LH and RH regions are attained at 7.8 and 9 GHz, and they are below −14 dB. Simulated radiation efficiency changes within 70 to 85%, while the overall one slightly exceeds 48 %. Comparison with the other similar periodic and CRLH LWAs showed that the developed nonuniform structure of antenna in a number of cases enabled obtaining the lower SLL as well as providing sufficient gain and quite a good efficiency for much smaller overall dimensions of the radiator.

REFERENCES

1. Deslandes, D. and K. Wu, "Single-substrate integration technique of planar circuits and waveguide filters," *IEEE Transactions on Microwave Theory and Techniques*, Vol. 51, No. 2, 593–596, 2003.
2. Hong, W., B. Liu, Y. Wang, Q. Lai, H. Tang, X. X. Yin, Y. D. Dong, Y. Zhang, and K. Wu, "Half mode substrate integrated waveguide: A new guided wave structure for microwave and millimeter wave application," *Proc. Joint 31st Int. Infrared Millimeter Waves Conf./14th Int. Terahertz Electronic Conf. 2006 (IRMMW-THz 2006)*, 219, 2006.
3. Jackson, D., C. Caloz, and T. Itoh "Leaky-wave antennas," *IEEE Proc.*, Vol. 100, No. 7, 2194–2206, July 2012.
4. Lyu, Y., X. Liu, P. Y. Wang, et al. Leaky-wave antennas based on non-cutoff substrate integrated waveguide supporting beam scanning from backward to forward," *IEEE Transactions on Antennas and Propagation*, Vol. 64, No. 6, 2155–2164, 2016.
5. Prakash, V., S. Kumawat, and P. Singh, "Design and analysis of full and half mode substrate integrated waveguide planar leaky wave antenna with continuous beam scanning in X-Ku band," *Frequenz*, 2019.
6. Agrawal, R., P. Belwal, and S. Gupta, "Asymmetric substrate integrated waveguide leaky wave antenna with open stop band suppression and radiation efficiency equalization through broadside," *Radioengineering*, Vol. 27, No. 2, 409–416, 2018.
7. Caloz, C., T. Itoh, and A. Rennings, "CRLH metamaterial leaky-wave and resonant antennas," *IEEE Antennas and Propagation Magazine*, Vol. 50, No. 5, 25–39, 2008.
8. Caloz, C. and T. Itoh, (n.d.), Novel microwave devices and structures based on the transmission line approach of meta-materials," *IEEE MTT-S International Microwave Symposium Digest*, 2003.
9. Sabahi, M. M., A. A. Heidari, and M. Movahhedi, "A compact CRLH circularly polarized leaky-wave antenna based on substrate-integrated waveguide," *IEEE Transactions on Antennas and Propagation*, Vol. 66, No. 9, 4407–4414, September 2018.
10. Dong, Y. and T. Itoh, 'Substrate integrated composite right-/left-handed leaky-wave structure for polarization-flexible antenna application," *IEEE Trans. Antennas Propag.*, Vol. 60, No. 2, 760–771, 2012.

11. Noumi, R., J. Machac, N. Boulajefan, and A. Gharsallah, "Development of SIW LWA from non-uniform CRLH unit cells with SLL reduction," *2018 18th Mediterranean Microwave Symposium (MMS)*, 2018.
12. Pourghorban Saghati, A., M. M. Mirsalehi, and M. H. Neshati,"A HMSIW circularly polarized leaky-wave antenna with backward, broadside, and forward radiation," *IEEE Antennas and Wireless Propagation Letters*, Vol. 13, 451–454, 2014.
13. Mohtashami, Y. and J. R. Mohasee, "A butterfly substrate integrated leaky wave antenna," *IEEE Trans. AntennasPropag.*, 2013.
14. Lai, A., C. Caloz, and T. Itoh, "Composite right/left-handed transmission line metamaterials," *IEEE Microwave Magazine*, Vol. 5, No. 3, 34–50, 2004.
15. Thomas, K. G. and G. Praveen, "A novel wideband circularly polarized printed antenna," *IEEE Transactions on Antennas and Propagation*, Vol. 60, No. 12, 5564–5570, 2012.
16. Caloz, C. and T. Itoh, *Electromagnetic Metamaterials: Transmission Line Theory and Microwave Applications: the Engineering Approach*, Wiley-IEEE Press, New York, NY, USA, 2006.
17. Henry, R. and M. Okoniewski, 'A broadside-scanning half-mode substrate integrated waveguide periodic leaky-wave antenna," *IEEE Antennas Wireless Propag. Lett.*, Vol. 13, 1429–1432, 2014.
18. Ostankov, A. V. and E. G. Khripunov, "Horn SIW-antenna with a special coplanar junction and dielectric lens for feeding of the planar leaky-wave antenna," *Radiostroenie*, No. 2, 1–26, 2020.
19. Jackson, D. R. and A. A. Oliner, *Leaky-wave Antennas' in Balanis, C.A., 'Modern Antenna Handbook'*, Ed. Hoboken, NJ, USA, Wiley, blue, 26 November 2007.
20. O'Connor, E. M., D. R. Jackson, and S. A. Long, "Extension of the Hansen-Woodyard condition for endfire leaky-wave antennas," *IEEE Antennas and Wireless Propagation Letters*, Vol. 9, 1201–1204, 2010.